Modulation of Proton-Coupled Electron Transfer Reactions by alpha-Helixes in the Lysine-Containing alpha-Helixes: alpha-Helixes Promoting Long-Range Electron Transfer

Long Chen, Xin Li, Xin Qin, Yuxin Xie, Nian Liu, Xiaohua Chen* and Yuxiang Bu*

Chongqing Key Laboratory of Theoretical and Computational Chemistry, School of Chemi
stry and Chemical Engineering, Chongqing University, Chongqing, 401331, P.R. China
School of Chemistry and Chemical Engineering, Shandong University, Jinan, 250100 Shandong, P. R. China

Supporting Information

1. Complete Reference

(86) M. J. Frisch, G. W. Trucks, H. B. Schlegel, G.E. Scuseria, M. A. Robb, J. R. Cheeseman, G. Scalmani, V. Barone, B. Mennucci, G. A. Prtersson, H. Nalatsyji, M.Caricato, X. Li, H. P. Hratchian, A. F. Izmaylov, J. Bloino, G. Zheng, J. L. Sonnenberg, M. Hada, M. Ehara, K. Toyota, R. Fukuda, J. Hasegawa, M. Ishida, T.Nakajima, Y. Honda, O. Kitao, H. Nakai, T. Vreven, J. A. Montgomery, Jr., J. E. Peralta, F. Ogliaro, M. Bearpark, J. J. Heyd, E. Brothers, K. N. Kudin, V. N. Staroverov, T. Keith, R. Kobayashi, J. Normand, K. Raghavachari, A. Rendell, J. C. Burant, S. S. Iyengar, J. Tomasi, M. Cossi, N. Rega, J. M. Millam, M. Klene, J. E. Knox, J. B. Cross, V. Bakken, C. Adamo, J. Jaramillo, R. Gomperts, R. E. Stratmann, O. Yazyev, A. J. Austin, R. Cammi, C. Pomelli, J. W. Ochterski, R. L. Martin, K. Morokuma, V. G. Zakrzewski, G. A. Voth, P. Salvador, J. J. Dannenberg, S. Dapprich, A. D. Daniels, O. Farkas, J. B. Foresman, J. V. Ortiz, J. Cioslowski, D. J. Fox, *Gaussian 09, Revision D.01;* Gaussian, Inc., Wallingford CT, 2013.

(87) Frisch, M. J.; Trucks, G. W.; Schlegel, H. B.; Scuseria, G. E.; Robb, M. A.; Cheeseman, J. R.; Scalmani, G.; Barone, V.; Petersson, G. A.; Nakatsuji, H.; Li, X.; Caricato, M.; Marenich, A. V.; Bloino, J.; Janesko, B. G.; Gomperts, R.; Mennucci, B.; Hratchian, H. P.; Ortiz, J. V.; Izmaylov, A. F.; Sonnenberg, J. L.; Williams-Young, D.; Ding, F.; Lipparini, F.; Egidi, F.; Goings, J.; Peng, B.; Petrone, A.; Henderson, T.; Ranasinghe, D.; Zakrzewski, V. G.; Gao, J.; Rega, N.; Zheng, G.; Liang, W.; Hada, M.; Ehara, M.; Toyota, K.; Fukuda, R.; Hasegawa, J.; Ishida, M.; Nakajima, T.; Honda, Y.; Kitao, O.; Nakai, H.; Vreven, T.; Throssell, K.; Montgomery, J. A., Jr.; Peralta, J. E.; Ogliaro, F.; Bearpark, M. J.; Heyd, J. J.; Brothers, E. N.; Kudin, K. N.; Staroverov, V. N.; Keith, T. A.; Kobayashi, R.; Normand, J.; Raghavachari, K.; Rendell, A. P.; Burant, J. C.; Iyengar, S. S.; Tomasi, J.; Cossi, M.; Millam, J. M.; Klene, M.; Adamo, C.; Cammi, R.; Ochterski, J. W.; Martin, R. L.; Morokuma, K.; Farkas, O.; Foresman, J. B.; Fox, D. J. *Gaussian 16*, revision B.01; Gaussian, Inc.: Wallingford, CT, 2016.

*The corresponding authors: Xiaohua Chen, chxh7@cqu.edu.cn
*The corresponding authors: Yuxiang Bu, byx@sdu.edu.cn

2. The assessing rate constants of the concerted proton-electron transfer reactions

The generalized transition state theory[s1-s4] is a fundamental approach to assessing the reaction rate of chemical reactions in proteins, the gas phase and the solution phase. Therefore, the rate constants (k_r) of the proton-coupled electron transfer reactions for all the Lys-containing α-helical systems are estimated by the equation (1s).

$$k_r = \frac{k_B T}{h} e^n \left(c^{\ominus}\right)^{1-n} \exp\left(\frac{\Delta S_f^{\neq}}{R}\right) \exp\left(-\frac{E_f}{RT}\right) \tag{1s}$$

In equal 1s, E_f is the forward energy barrier and $\Delta S_f^{\neq}$ is forward activation entropy. Both are obtained from the Gaussian 09/16 output files after the harmonic vibrational analyses at the B3LYP/6-31+G(d,p) theory of level.

In the proton-coupled electron transfer reactions, both proton transfer and electron transfer occur at the same time. Therefore, the rate constant (k_{ET}) of electron transfer is not be lower than or approximately equal to the rate constant (k_r) of the corresponding proton-coupled electron transfer reaction. k_{ET} be described by the semiclassical theory of the Marcus−Hush−Levich formulism (2s)[s5-s12].

$$k_{\mathrm{ET}} = \frac{2\pi}{\hbar} \frac{1}{\sqrt{4\pi\lambda k_b T}} \left|H_{DA}\right|^2 \exp\left(-\frac{(\lambda + \Delta G_r)^2}{4\lambda k_b T}\right) \tag{2s}$$

In this expression, λ is the nuclear reorganization energy accompanying electron transfer, H_{DA} is electronic coupling matrix element between the donor and acceptor, ΔG_r is reaction free energy, $\hbar$ is Planck's constant, k_b is Boltzmann's constant and T is temperature.

In addition, the nuclear reorganization energy (λ) can be obtained by the equation 3s.

$$\Delta G_f^{\neq} = \frac{(\lambda + \Delta G_r)^2}{4\lambda} \tag{3s}$$

In the equation 3s, $\Delta G_f^{\neq}$ is the forward free energy barrier, which is the difference in free energy between reactant and transition state. The reaction free energy (ΔG_r) is the difference in free energy between reactant and product.

Then, the electronic coupling matric element (H_{AD}) can be rough calculated according to the equation between k_r and k_{ET}. Therefore, we can assess the decay factor (β) of electronic coupling matric element (H_{AD}) with increased distance for electron transfer along the α-helix using equation 4s[s5-s12].

$$H_{DA} = H_{DA}^0 \exp(-\beta_{\mathrm{ET}} \Delta r) \tag{4s'}$$

Equation 4s' can be changed into 4s.

$$\beta_{\mathrm{ET}} = -\frac{1}{\Delta r}\ln\left(\frac{H_{DA}}{H_{DA}^{0}}\right) \tag{4s}$$

In the expression of 4s, Δr is the shortest distance between the donor and the acceptor, H_{DA} is electronic coupling matrix element between the donor and the acceptor, and H_{DA}^{0} is the electronic coupling matrix element for the case that the donor is close to the acceptor. As the Koopmans theorem (KT) theory, the electronic coupling H_{DA}^{0} is related to the energies of the frontier molecular orbitals (MOs) using the structure of the corresponding radical, and it is estimated by equation 5s[s13,s14]

$$H_{DA}^{0} = \frac{\varepsilon_{\mathrm{LUMO+n}} - \varepsilon_{\mathrm{SOMO}}}{2} \tag{5s}$$

Where ε_i is the energy of the singly occupied MO (SOMO) or the nth lowest unoccupied MO (LUMO+n). SOMO is an electron donor and LUMO+n is an acceptor.

References:

(s1) Eyring, H. *Chem. Rev.* **1935**, *17*, 65–77.

(s2) Eyring, H.; Stearn, A. E. *Chem. Rev.* **1939**, *24*, 253–270.

(s3) Pu, J.; Gao, J.; Truhlar, D. G. *Chem. Rev.* **2006**, *106*, 3140–3169.

(s4) Gao, J.; Ma, S.; Major, D. T.; Nam, K.; Pu, J.; Truhlar, D. G. *Chem. Rev.* **2006**, *106*, 3188–3209.

(s5) Marcus, R. A. *J. Chem. Phys.* **1965**, *43*, 679–701.

(s6) Hush, N. S. *Trans. Faraday Soc.* **1961**, *57*, 557–580.

(s7) Levich, V. G. *Adv. Electrochem. Electrochem. Eng.* **1966**, *4*, 249–371.

(s8) Marcus, R. A.; Sutin, N. *Biochim. Biophys. Acta* **1985**, *811*, 265–322.

(s9) Costentin, C.; Evans, D. H.; Robert, M.; Savéant, J.-M.; Singh, P. S. *J. Am. Chem. Soc.* **2005**, *127*, 12490–12491.

(s10) Schrauben, J. N.; Cattaneo, M.; Day, T. C.; Tenderholt, A. L.; Mayer, J. M. *J. Am. Chem. Soc.* **2012**, *134*, 16635−16645.

(s11) Nelsen, S. F.; Weaver, M. N.; Bally, T.; Yamazaki, D.; Komatsu, K.; Rathore, R. *J. Phys. Chem. A* **2007**, *111*, 1667–1678.

(s12) Datta, A.; Mohakud, S.; Pati, S. K. J. *Mater. Chem.* **2007**, *17*, 1933–1938.

(s13) Nelsen, S. F.; Weaver, M. N.; Bally, T.; Yamazaki, D.; Komatsu, K.; Rathore, R. *J. Phys. Chem. A* **2007**, *111*, 1667–1678.

(s14) Datta, A.; Mohakud, S.; Pati, S. K. J. *Mater. Chem.* **2007**, *17*, 1933–1938.

cam-B3LYP/6-31+G(d,p)

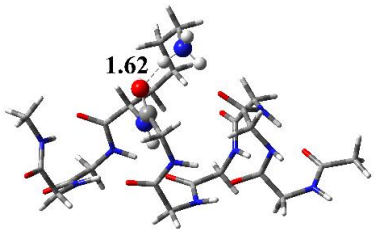

G_2-K-G_6-r

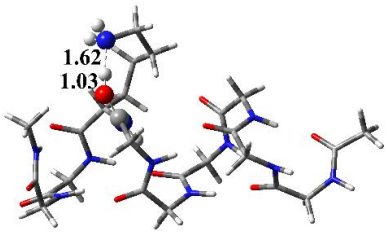

G_2-K-G_6-ts (23.62/23.77)

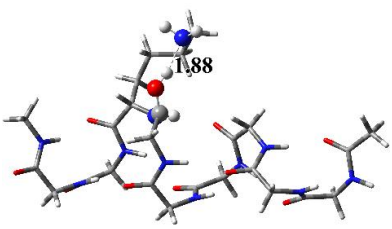

G_2-K-G_6-p

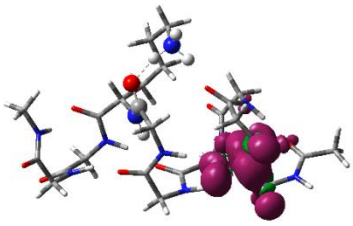

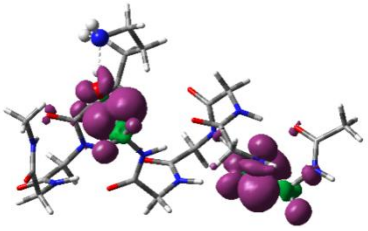

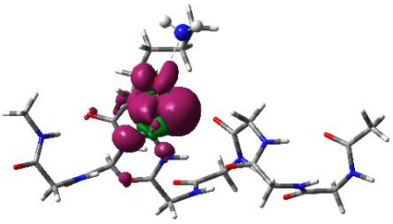

M062X/6-31+G(d,p)

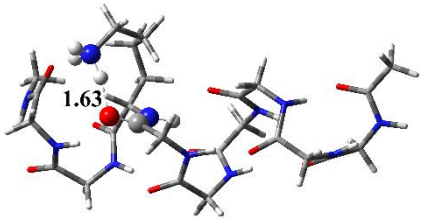

G_2-K-G_6-r

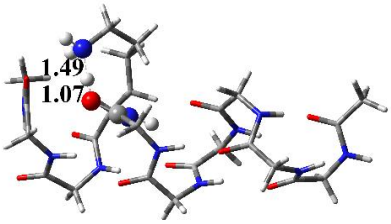

G_2-K-G_6-ts (8.63/16.58)

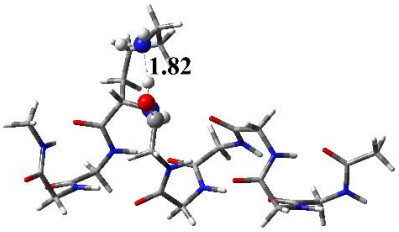

G_2-K-G_6-p

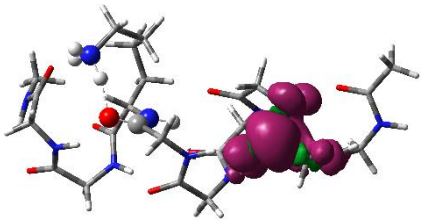

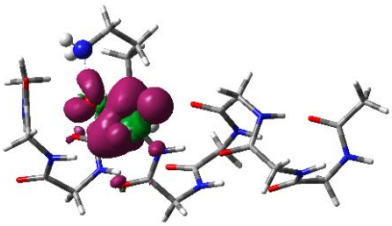

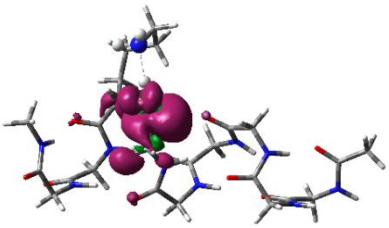

BhandLYP/6-31+G(d,p)

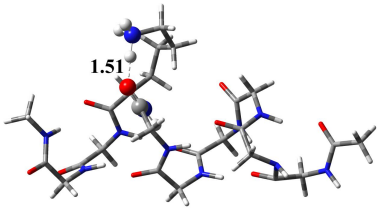

G_2-K-G_6-r

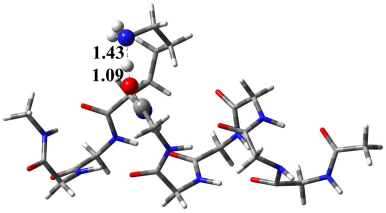

G_2-K-G_6-ts (1.21/17.34)

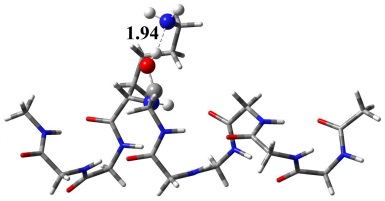

G_2-K-G_6-p

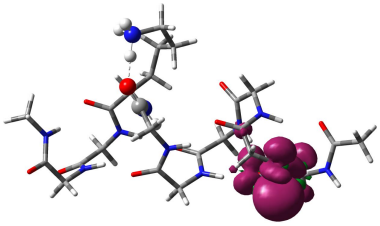

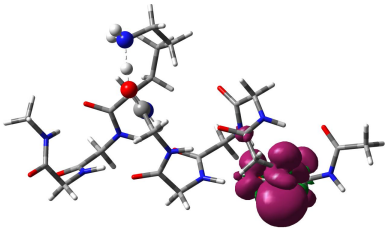

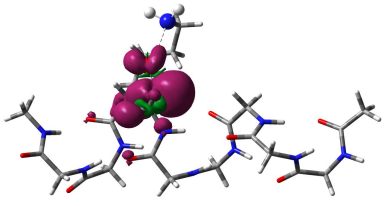

B3LYP/6-31+G(d,p)

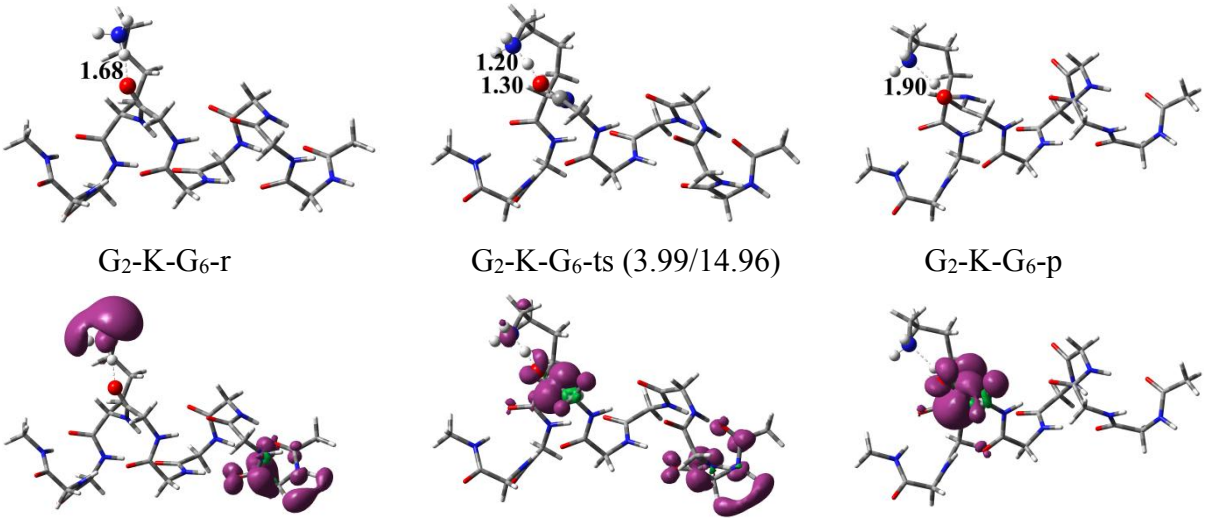

Figure S1. The comparison of optimization results from cam-B3LYP, M06-2X, BhandLYP and B3LYP for the the G_2-K^1-G_6 system.

To verify the reliability of B3LYP/6-31+G(d,p) for examining the PCET reactions of the G_2-K-G_{n-3} systems, we also carried out the other two DFT functionals, BhandLYP, cam-B3LYP and M06-2X, with the same basis set to optimize the reactant, transition state and product of G_2-K-G_6. The cam-B3LYP and M06-2X functionals conforms that the stable conformation for the reactant of G_2-K^1-G_6 is the ammonium group forming two H-bonds with the main chain, in which excess electron entirely resides at the N-terminus of α-helix. The three functionals obtained the similar transition state structure to the B3LYP. The cam-B3LYP functional reveals that the spin density is delocalized over both the N-terminus and the neighboring peptide bond unit in the transition state, which is in line with the result obtained by the B3LYP optimization. However, excess electron mainly localizes on the neighboring peptide bond unit for M06-2X and on the N-terminus for BhandLYP. The geometrical structure and the distribution of excess electron for the product obtained from the three functionals is consistent with the B3LYP functional. Therefore, the three functionals reveal that the proton/electron transfer reactions of G_2-K-G_6 takes place through the same vertical proton-coupled electron transfer mechanism with proton transfer from the side chain of K to the O-atom of the neighboring peptide bond and electron transfer from the N-terminus to the neighboring peptide bond at same time. These results indicate that the conformations of reactant is effected by the different functionals and the most stable double-H-binding conformation is obtained by the other DFT functionals. However, the single-H-binding conformation can not be achieved by cam-B3LYP and M06-2X functionals. In the double-H-binding conformation of G_2-K-G_6, the spin density mainly localizes on the N-terminus of α-helix, which can be used to examine the electron transport ability of α-helix. The forward/backward energy barrier (1.21/17.34) obtained by BhandLYP is consistent with that (3.99/14.96) obtained by B3LYP. In reality, the energy barrier is

changed with the different functionals, some functionals give the higher energy barriers than the B3LYP functional because of the difference in considering the long-range interactions. However, in this work, our goal is to obtain the changing tendency in the rate constant of PCET with the increase length of α-helix and don't achieve the accurate energy barriers and rate constant of PCET of the G_2-K-G_{n-3} and G_{n-3}-K-G_2 systems.

3. Tables

Table S1. Forward Activation Entropy ($\Delta S_f^{\neq}$), Reorganization Energy (λ), Rate Constant (k_r) of the Forward Obtained from the Transition State Theory, ET Distance along the α-Helix (r), Electronic Coupling Matrix Element (H_{AD}) and Decay Factor of H_{AD} with Increased Distance (β) for G_2-K-G_{n-3} (n=5, 6, 7, 8, 9, 11, 13).

	$\Delta S_f^{\neq}$ (cal/mol)	λ (eV)	k_r (Dy, s^{-1})	r (Å)	H_{AD} (cm^{-1})	β
G_2-K-G_2	-13.13	1.65	3.13×10^{9}	4.94	67.9	1.15
G_2-K-G_3	-6.83	1.16	1.19×10^{12}	6.12	131.1	0.72
G_2-K-G_4	-15.17	1.41	2.24×10^{11}	7.92	111.5	0.57
G_2-K-G_5	-29.47	1.13	1.46×10^{11}	7.75	100.1	0.60
G_2-K-G_6	-12.22	1.38	6.12×10^{10}	10.02	94.5	0.47
G_2-K-G_8	-14.98	1.34	8.59×10^{10}	12.14	97.6	0.42
G_2-K-G_{10}	-35.30	1.34	9.12×10^{9}	15.63	73.6	0.34

Table S2. Forward Activation Entropy ($\Delta S_f^{\neq}$), Reorganization Energy (λ), Rate Constant (k_r) of the Forward Obtained from the Transition State Theory, ET Distance along the α-Helix (r), Electronic Coupling Matrix Element (H_{AD}) and Decay Factor of H_{AD} with Increased Distance (β) for the Proton/Electron Acceptor being the First Neighboring Peptide Bond (G_2-K^1-G_{n-3}-ts) and the Fourth Peptide Bond (G_2-K^4-G_{n-3}-ts) with the Ammonium Group Interacting with the Main Chain via Two Hydrogen Bonds.

TS	$\Delta S_f^{\neq}$ (cal/mol)	λ (eV)	k_r (s^{-1})	r (Å)	H_{DA} (cm^{-1})	β
G_2-K^1-G_5	-11.28	1.27	1.51×10^{10}	7.52	77.4	0.71
G_2-K^1-G_6	-10.35	1.28	5.20×10^{9}	9.82	67.9	0.54
G_2-K^1-G_8	-11.85	0.79	4.31×10^{11}	11.64	104.8	0.40
G_2-K^1-G_{10}	-8.31	0.63	6.68×10^{11}	15.18	104.5	0.29
G_2-K^4-G_5	-12.26	1.19	4.32×10^{11}	4.82	116.1	1.04
G_2-K^4-G_6	-8.61	1.02	8.23×10^{11}	5.95	121.3	0.82
G_2-K^4-G_8	-7.10	0.97	5.64×10^{11}	7.80	114.7	0.60
G_2-K^4-G_{10}	-5.57	0.92	5.53×10^{11}	11.07	112.4	0.41

Table S3. Forward Energy Barriers (E_f), Backward Energy Barriers (E_b) and Forward Rate Constant (k_r) of the PCET Reactions in the G_2-K-G_{n-3}-A and G_2-K^4-G_{n-3}-A Systems with the Zero-Point Energy Corrections.

	G_2-K-G_2-A	G_2-K-G_6-A	G_2-K-G_8-A	G_2-K-G_{10}-A
E_f (kcal/mol)	6.25	4.53	4.59	4.52
E_b (kcal/mol)	15.79	17.37	17.56	17.68
k_r(s^{-1})	3.05×10^{8}	5.88×10^{9}	6.26×10^{9}	1.84×10^{10}
	G_2-K^4-G_5-A	G_2-K^4-G_6-A	G_2-K^4-G_8-A	G_2-K^4-G_{10}-A
E_f (kcal/mol)	6.75	4.72	4.17	3.45
E_b (kcal/mol)	18.26	17.64	17.72	13.71
k_r(s^{-1})	1.95×10^{7}	3.54×10^{8}	1.30×10^{10}	1.46×10^{11}

Table S4. Forward Energy Barrier (E_f), Backward Energy Barrier (E_b), Forward Activation Entropy ($\Delta S_f^{\neq}$), Forward Rate Constant (k_r) of the PCET Reactions Obtained from the Transition State Theory and Decay Factor (β_{ET}) of Electronic Coupling Matric Element (H_{AD}) with Increased Distance for G_{n-3}-K-G_2. E_f and E_b are corrected by the Zero-Point Energies.

	E_f (kcal/mol)	E_b (kcal/mol)	$\Delta S_f^{\neq}$ (cal/mol)	k_r (s^{-1})	β
G_4-K-G_2	3.15	22.08	-8.11	1.40×10^9	1.12
G_6-K-G_2	3.90	24.76	-6.37	9.45×10^8	1.11
G_8-K-G_2	4.30	27.57	-0.17	1.10×10^{10}	1.10
G_{10}-K-G_2	4.65	21.18	-1.01	3.96×10^9	1.15

Table S5. Forward Energy Barrier (E_f) and Backward Energy Barrier (E_b) for G_2-K-G_{n-3} (n=5, 6, 7, 8, 9, 11, 13) with the Ammonium Group Interacting with the Main Chain via a Hydrogen Bond in Diethyl Ether (Dielectric Constant, ε = 4.335) Continuum Solvents at the B3LYP/6-311+G(d,p) Level by Using the Conductor-Like Polarizable Continuum Model (CPCM). E_f and E_b are corrected by the Zero-Point Energies.

CPCM	G_2-K-G_2	G_2-K-G_3	G_2-K-G_4	G_2-K-G_5	G_2-K-G_6	G_2-K-G_8	G_2-K-G_{10}
E_f (kcal/mol)	-0.51	-1.14	-2.42	4.28	7.47	7.30	9.20
E_b (kcal/mol)	15.40	16.70	16.26	24.93	26.37	26.27	23.10

Table S6. Forward Energy Barrier (E_f) and Backward Energy Barrier (E_b) for Proton/Electron Acceptor Being the First Neighboring Peptide Bond (G_2-K^1-G_{n-3}-ts) and the Fourth Peptide Bond (G_2-K^4-G_{n-3}-ts) with the $-NH_3^+$ Group Interacting with the Main Chain via Two H-bonds in Diethyl Ether (Dielectric Constant, ε = 4.335) Continuum Solvents at the B3LYP/6-311+G(d,p) Level by Using the Conductor-Like Polarizable Continuum Model (CPCM). E_f and E_b are corrected by the Zero-Point Energies.

CPCM	G_2-K^1-G_5-ts	G_2-K^1-G_6-ts	G_2-K^1-G_8-ts	G_2-K^1-G_{10}-ts
E_f (kcal/mol)	9.49	6.01	5.79	7.77
E_b (kcal/mol)	17.87	17.21	17.17	15.87
	G_2-K^4-G_5-ts	G_2-K^4-G_6-ts	G_2-K^4-G_8-ts	G_2-K^4-G_{10}-ts
E_f (kcal/mol)	5.45	5.62	4.66	6.79
E_b (kcal/mol)	19.12	18.89	18.26	19.99

Table S7. Forward Energy Barrier (E_f) and Backward Energy Barrier (E_b) for the G_2-K-G_{n-3}-A and G_2-K^1-G_{n-3}-A (via G_2-K^4-G_{n-3}-ts) Systems in Diethyl Ether (Dielectric Constant, ε = 4.335) Continuum Solvents at the B3LYP/6-311+G(d,p) Level by Using the Conductor-Like Polarizable Continuum Model (CPCM). E_f and E_b are corrected by the Zero-Point Energies.

CPCM	G_2-K-G_2-A	G_2-K-G_6-A	G_2-K-G_8-A	G_2-K-G_{10}-A
E_a (kcal/mol)	0.28	0.04	-0.08	-0.19
E_b (kcal/mol)	15.35	18.90	17.45	17.34
	G_2-K^4-G_5-A-ts	G_2-K^4-G_6-A-ts	G_2-K^4-G_8-A-ts	G_2-K^4-G_{10}-A-ts
E_a (kcal/mol)	3.31	2.34	3.79	2.26
E_b (kcal/mol)	19.71	19.84	18.57	16.65

4. The optimized structures for PCET reactions with the spin density distributions

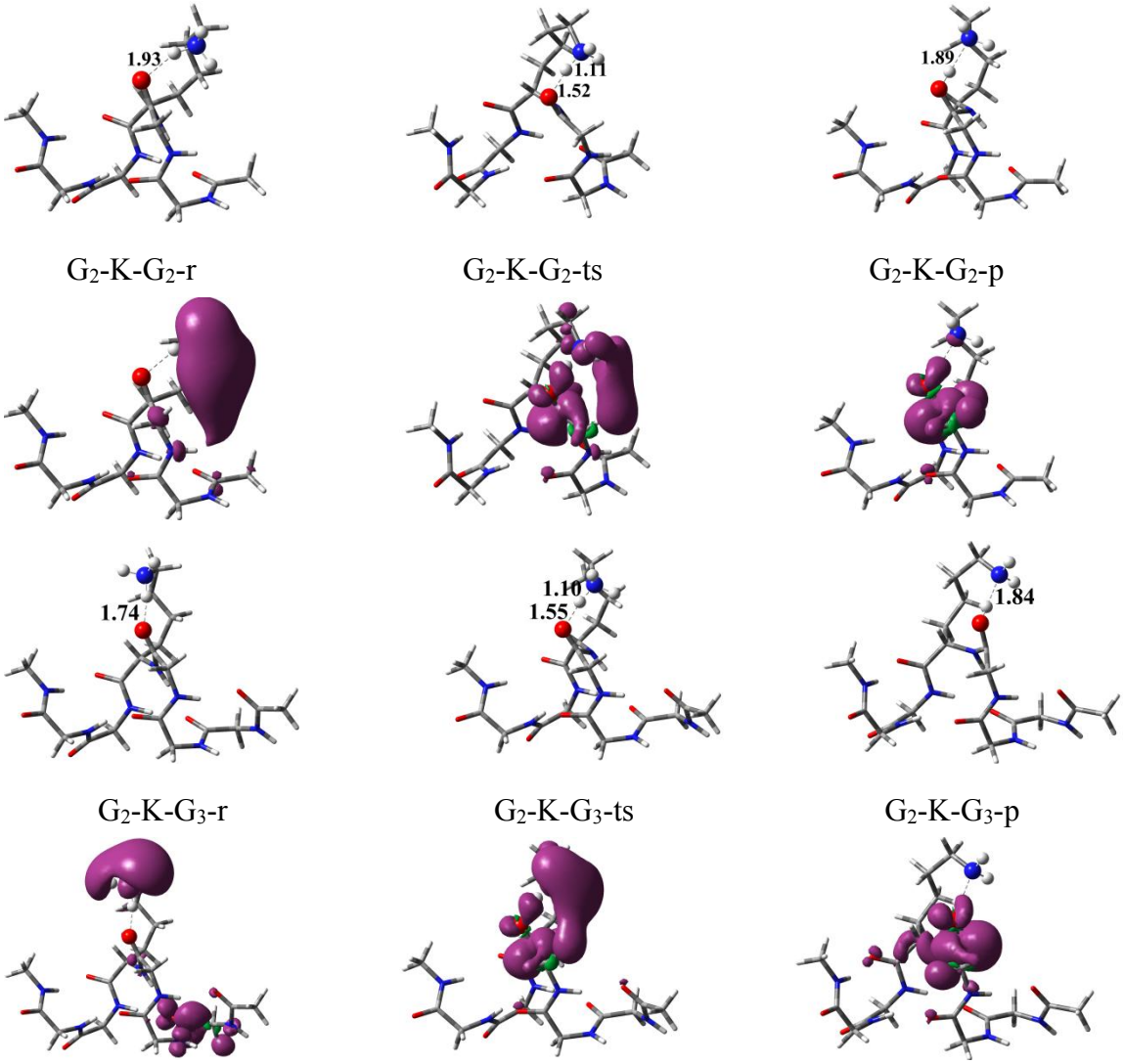

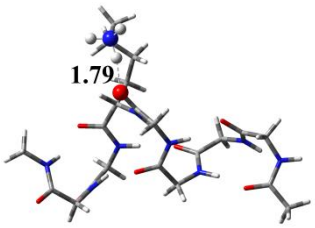

G_2-K-G_4-r

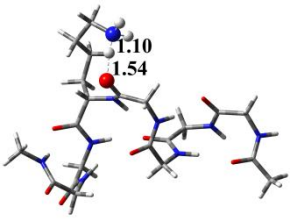

G_2-K-G_4-ts

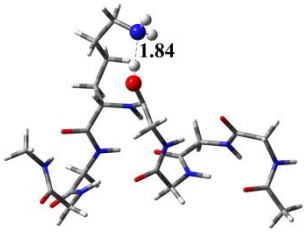

G_2-K-G_4-p

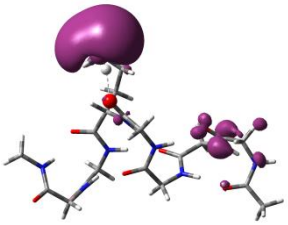

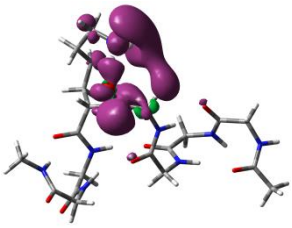

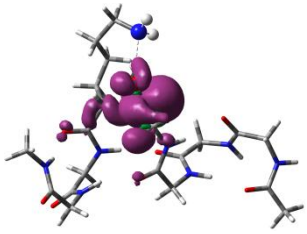

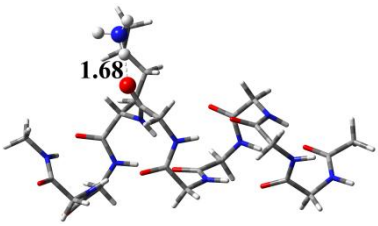

G_2-K-G_6-r

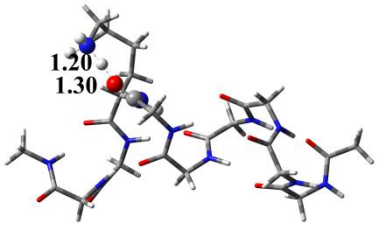

G_2-K-G_6-ts

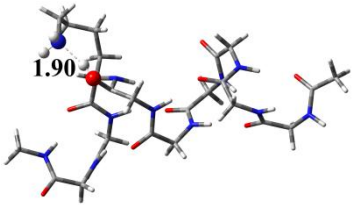

G_2-K-G_6-p

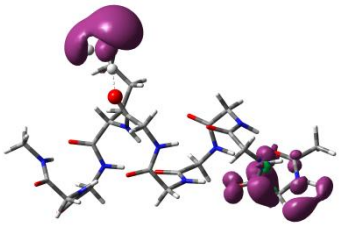

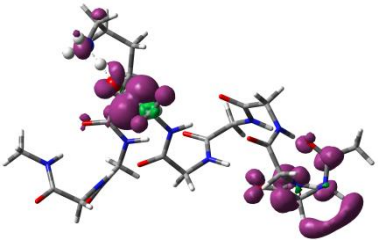

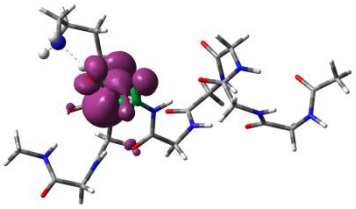

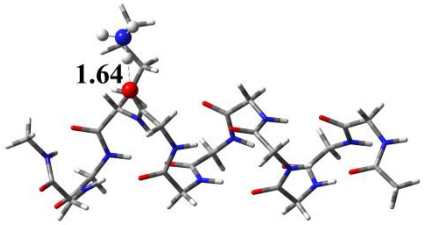

G_2-K-G_8-r

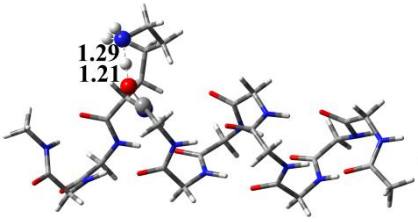

G_2-K-G_8-ts

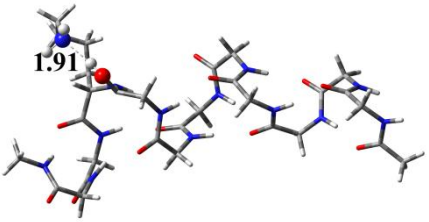

G_2-K-G_8-p

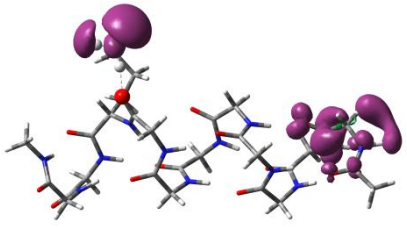

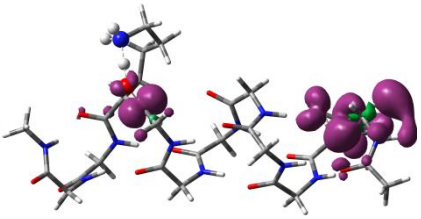

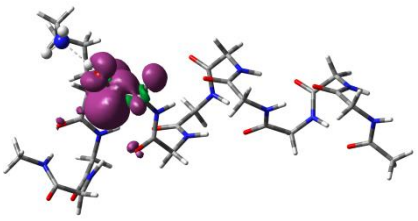

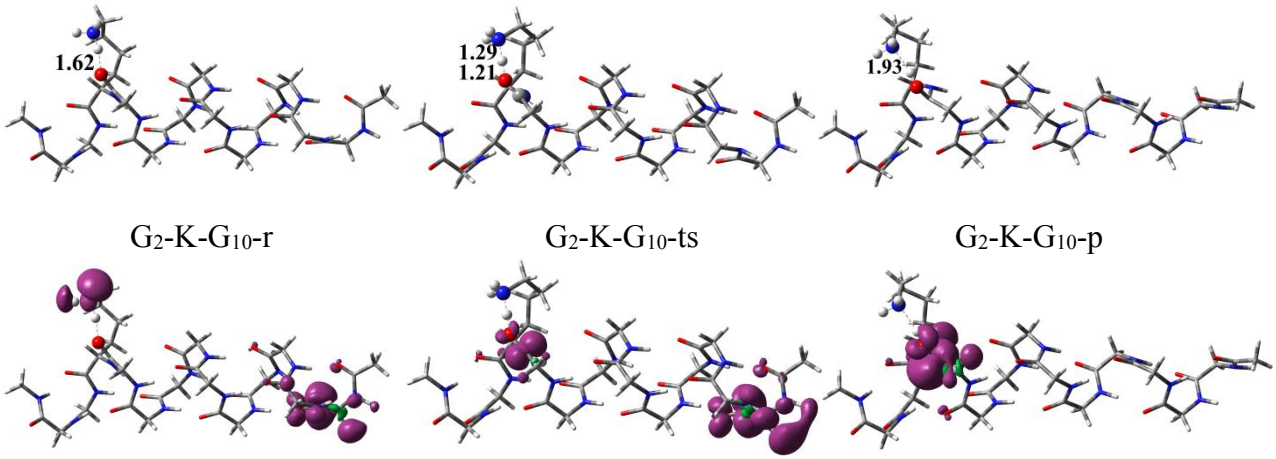

Figure S2. The structures of reactants, transition states, products for G_2-K-G_{n-3} (n=5, 6, 7, 9, 11, 13) and the corresponding distributions of spin densities for the initial structures with the ammonium group interaction with the helical framework via only a hydrogen bond.

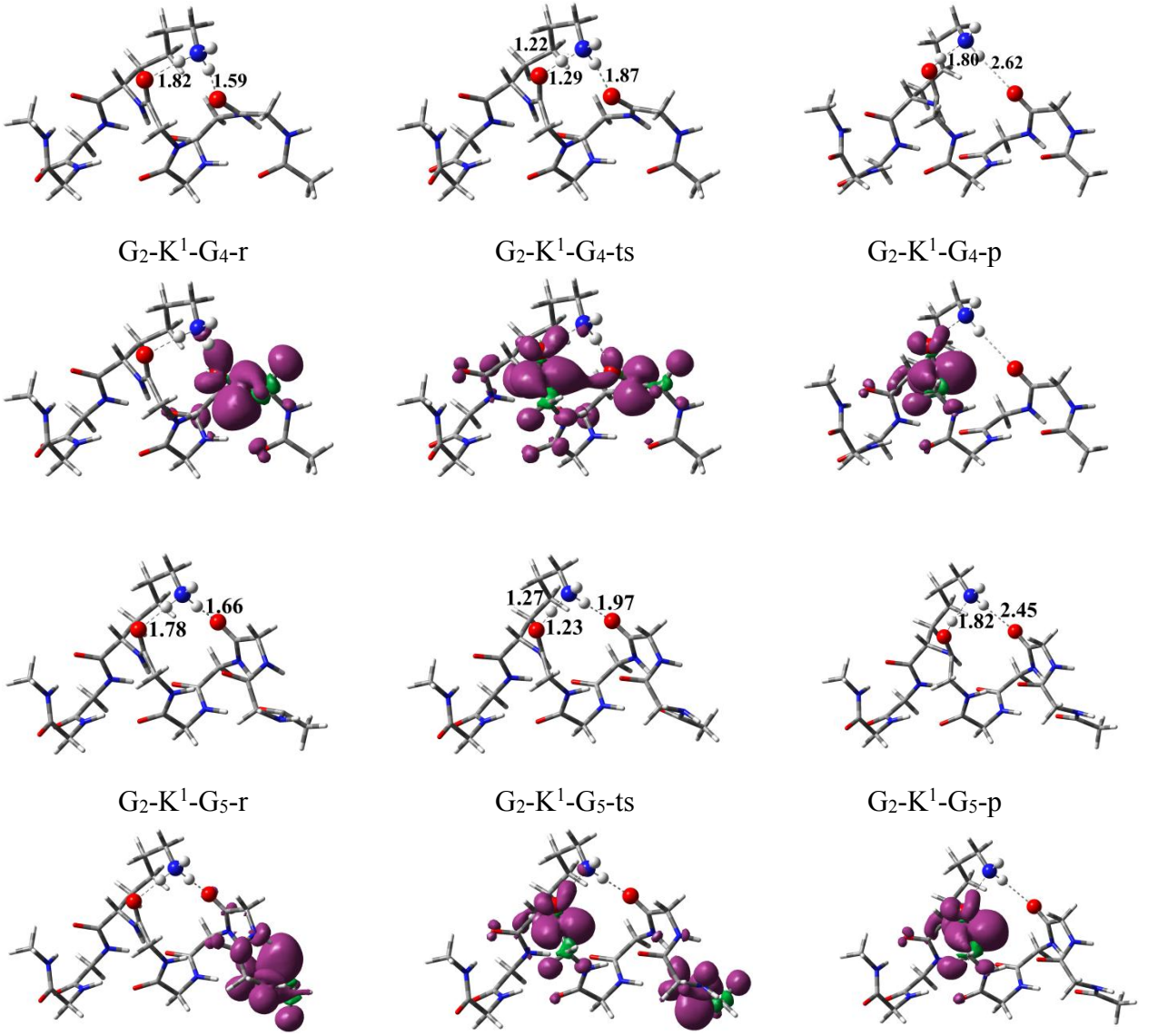

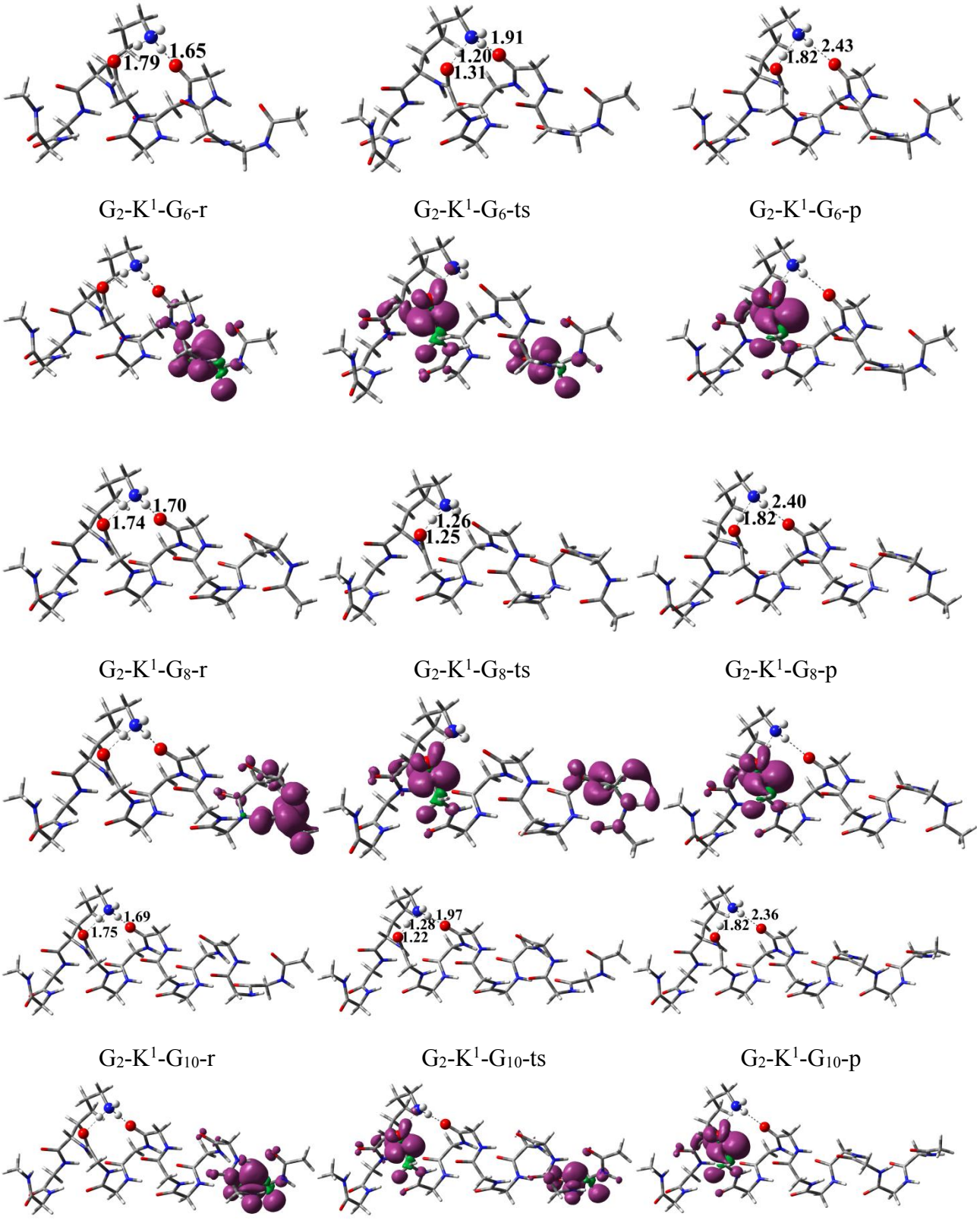

Figure S3. The structures of reactants, transition states, products for the first peptide bond acting as proton/electron acceptors in G_2-K-G_{n-3} (n=7, 8, 9, 11, 13) and the corresponding distributions of spin densities for the initial structures with the ammonium group interaction with the helical framework via two hydrogen bonds obtained at the B3LYP/6-31+G(d,p) level of theory.

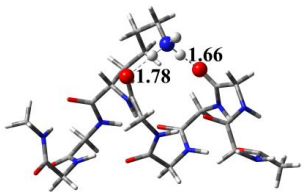

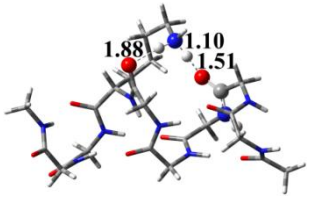

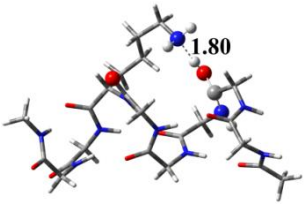

G_2-K^1-G_5-r

G_2-K^4-G_5-ts

G_2-K^4-G_5-p

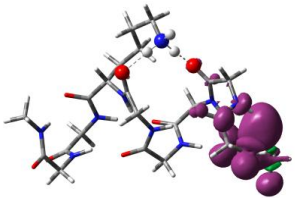

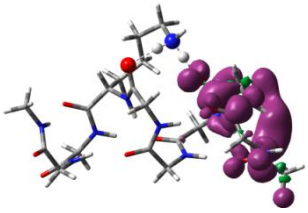

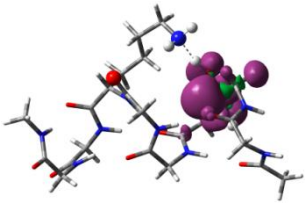

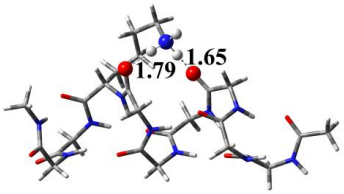

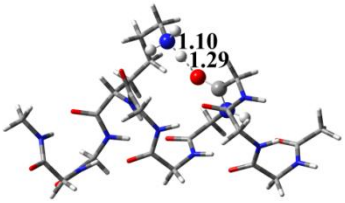

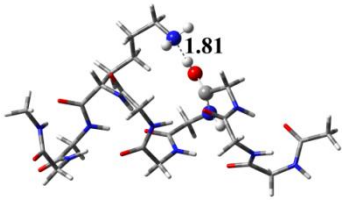

G_2-K^1-G_6-r

G_2-K^4-G_6-ts

G_2-K^4-G_6-p

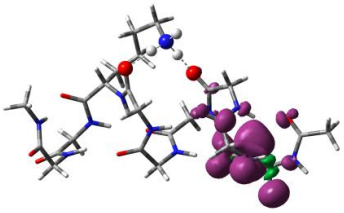

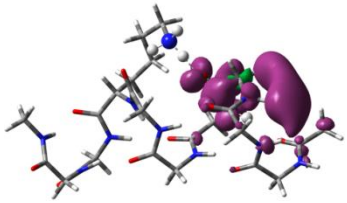

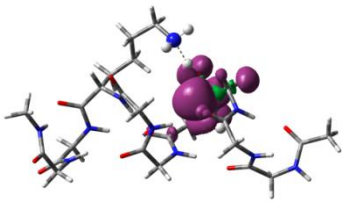

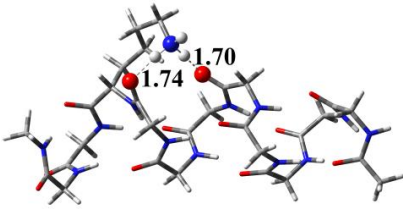

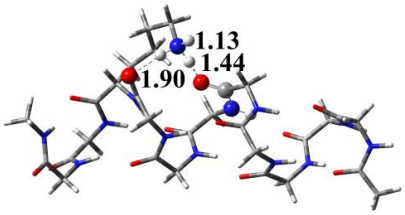

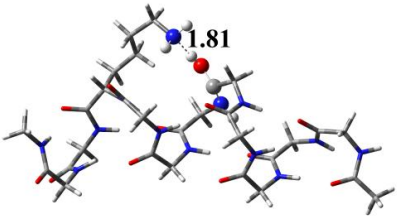

G_2-K^1-G_8-r

G_2-K^4-G_8-ts

G_2-K^4-G_8-p

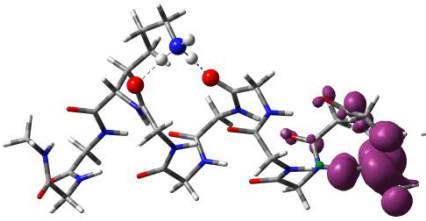

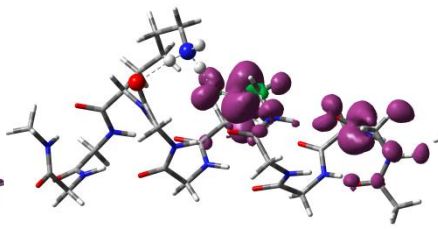

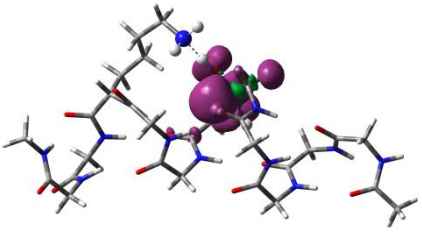

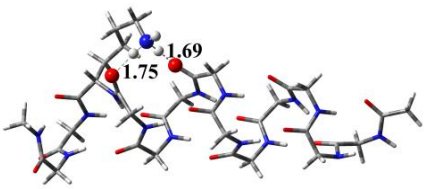

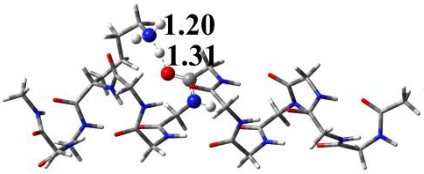

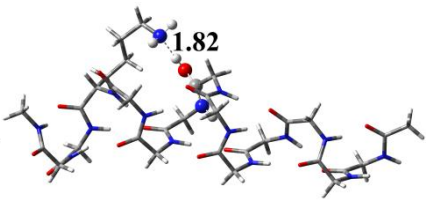

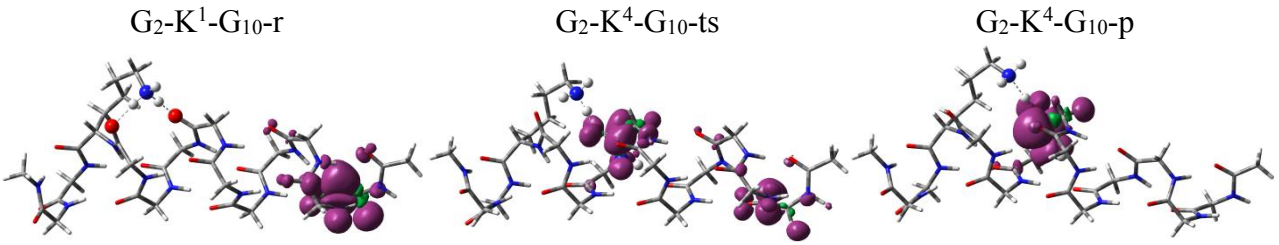

Figure S4. The structures of reactants, transition states, products for the fourth peptide bond acting as proton/electron acceptors in G_2-K-G_{n-3} (n=8, 9, 11, 13) and the corresponding distributions of spin densities for the initial structures with the ammonium group interaction with the helical framework via two hydrogen bonds obtained at the B3LYP/6-31+G(d,p) level of theory.

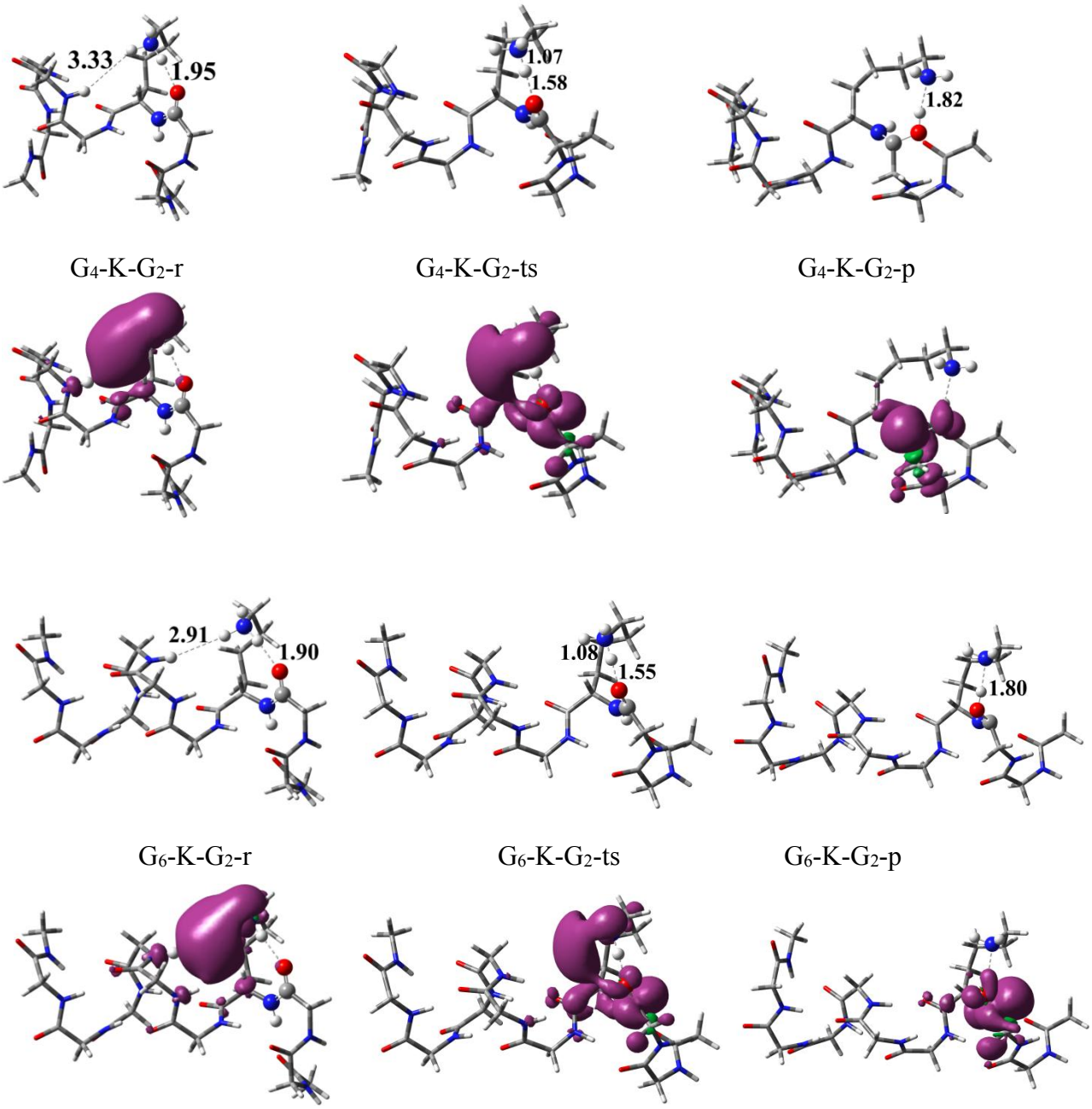

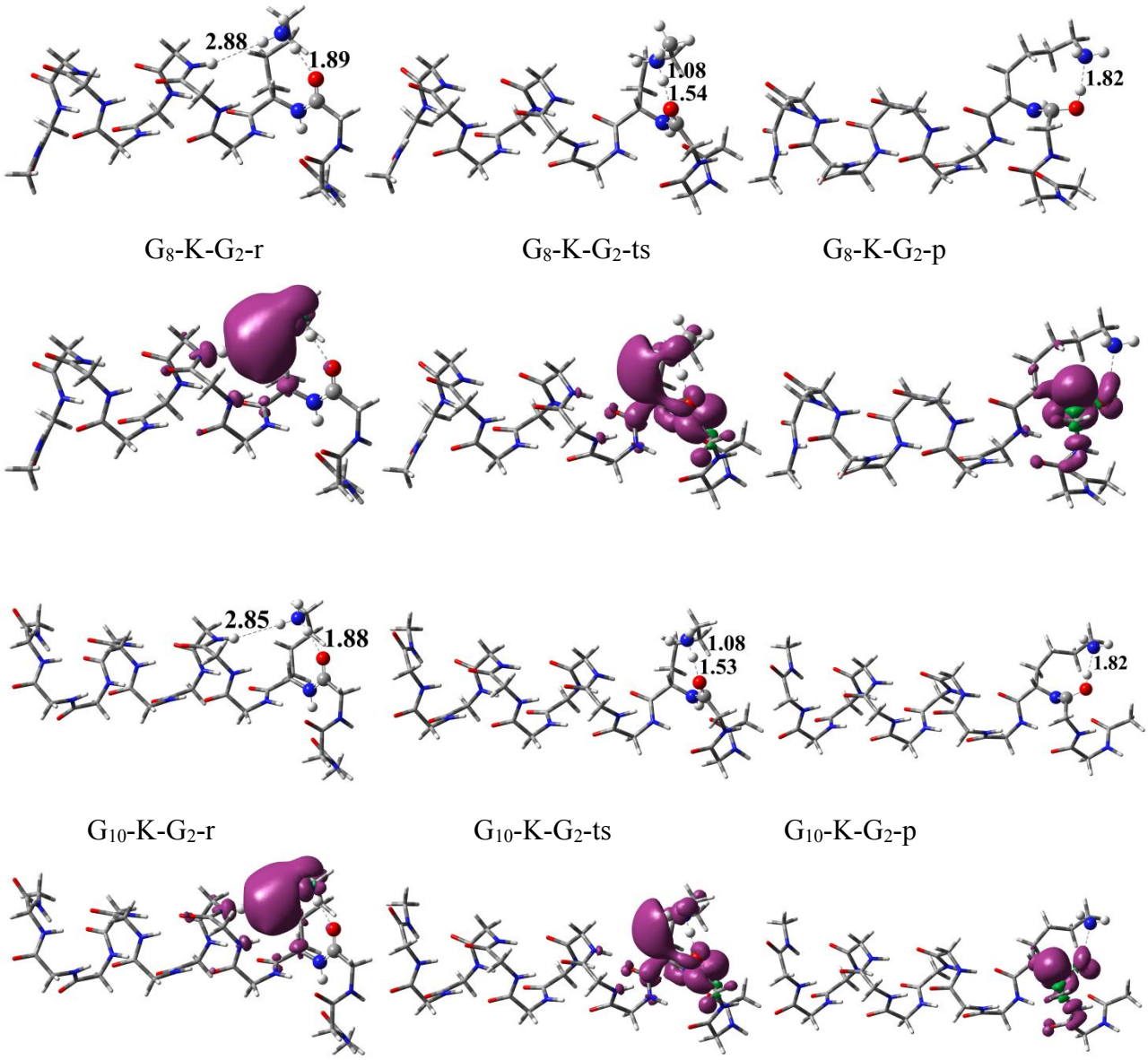

Figure S5. The structures of reactants, transition states, products for K residing at the third residue from the C-terminus, named as G_{n-3}-K-G_2 (n=7, 9, 11, 13) and the corresponding distributions of spin densities obtained at the B3LYP/6-31+G(d,p) level of theory.

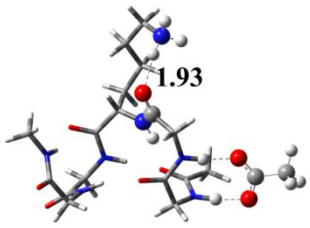

G_2-K-G_2-A-r

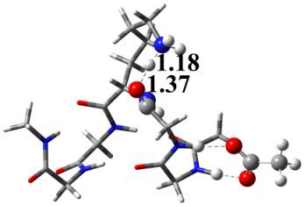

G_2-K-G_2-A-ts

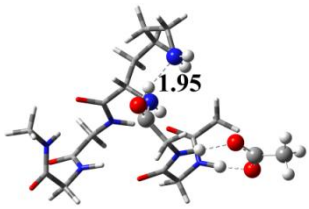

G_2-K-G_2-A-p

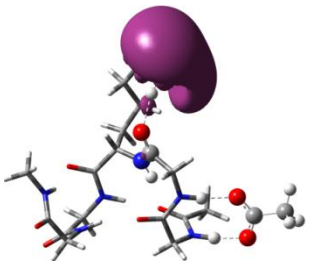

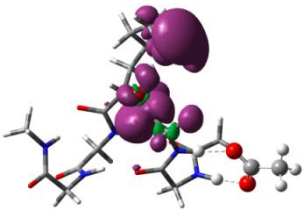

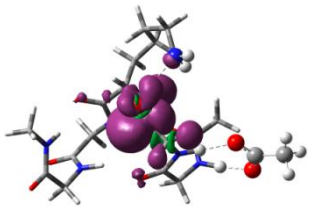

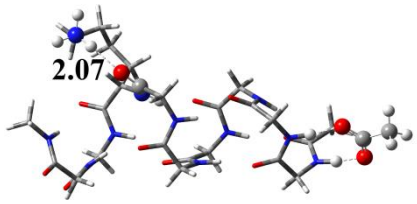

G_2-K-G_6-A-r

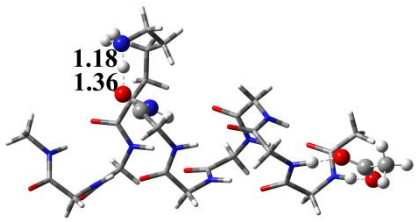

G_2-K-G_6-A-ts

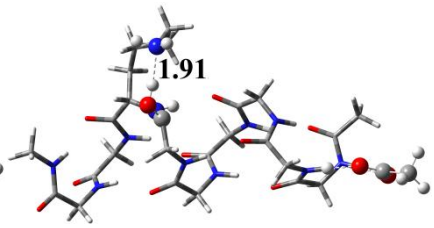

G_2-K-G_6-A-p

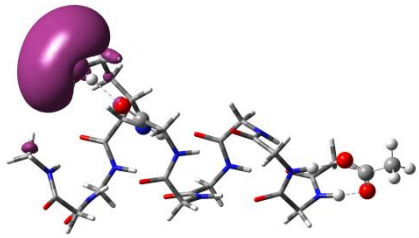

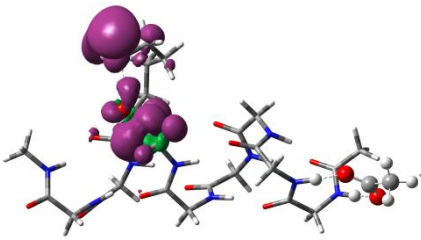

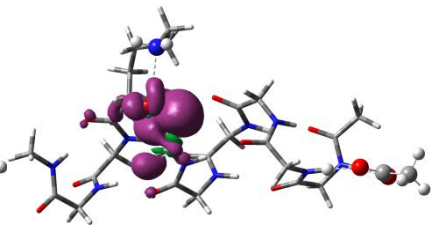

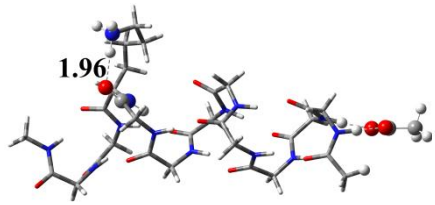

G_2-K-G_8-A-r

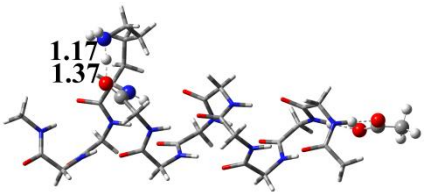

G_2-K-G_8-A-ts

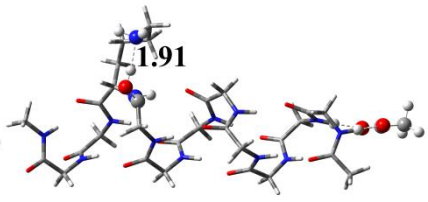

G_2-K-G_8-A-p

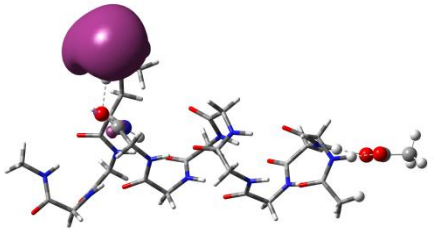

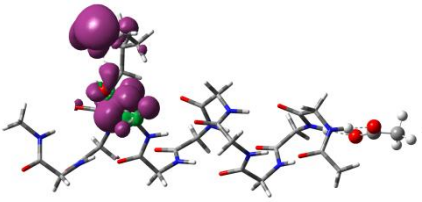

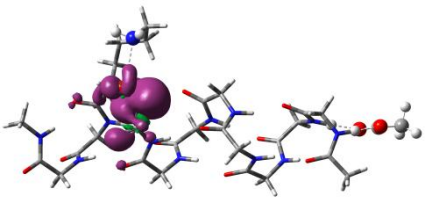

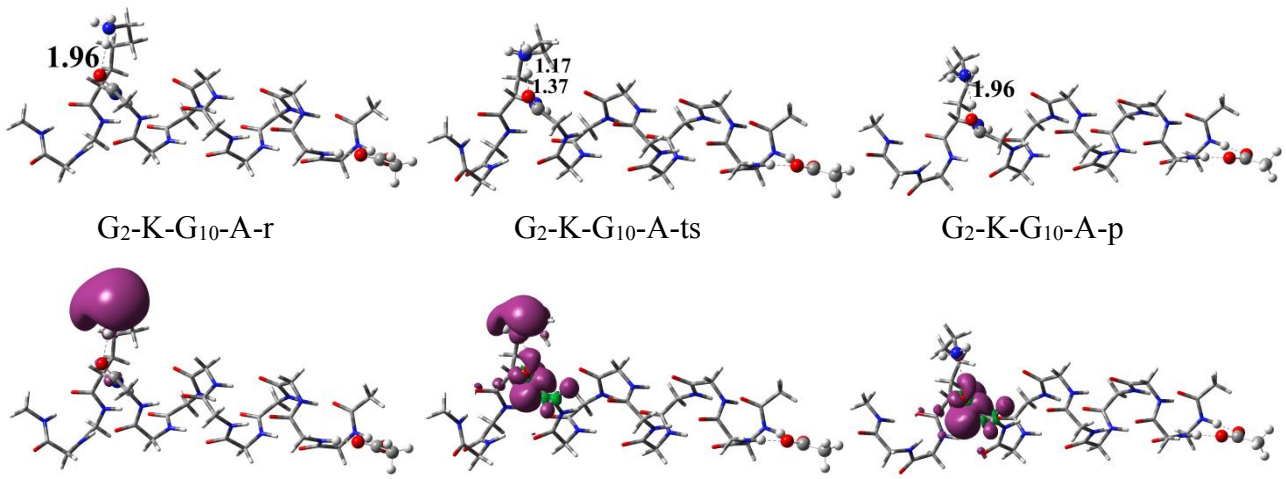

G_2-K-G_{10}-A-r G_2-K-G_{10}-A-ts G_2-K-G_{10}-A-p

Figure S6. The structures of reactants, transition states, products for G_2-K-G_{n-3}-A (n=5, 9, 11, 13) and the corresponding distributions of spin densities for the initial structures with the ammonium group interaction with the helical framework via only a hydrogen bond. According these cases, we examined the influence of the capping (the negative groups including the side chains of Asp, Glu) on the PCET reactions in the G_2-K-G_{n-3} systems obtained at the B3LYP/6-31+G(d,p) level of theory.

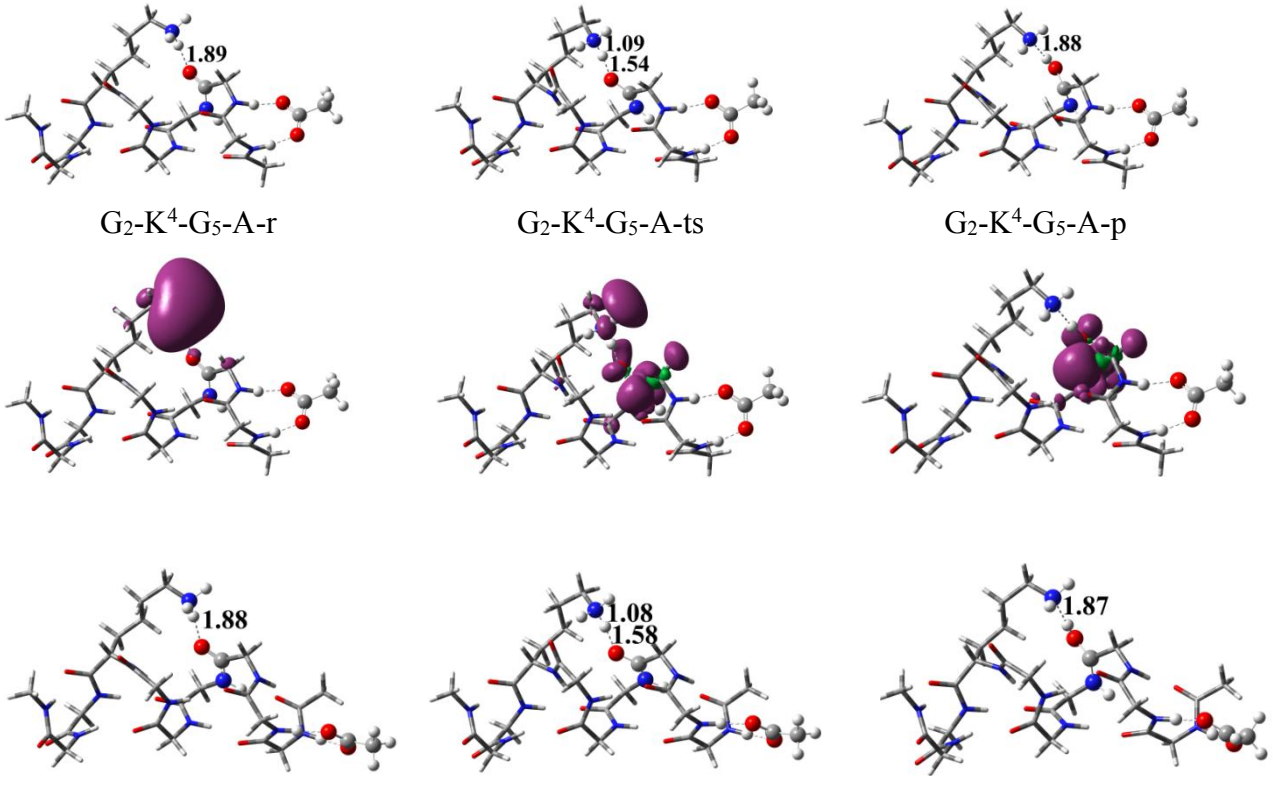

G_2-K^4-G_5-A-r G_2-K^4-G_5-A-ts G_2-K^4-G_5-A-p

G_2-K^4-G_6-A-r G_2-K^4-G_6-A-ts G_2-K^4-G_6-A-p

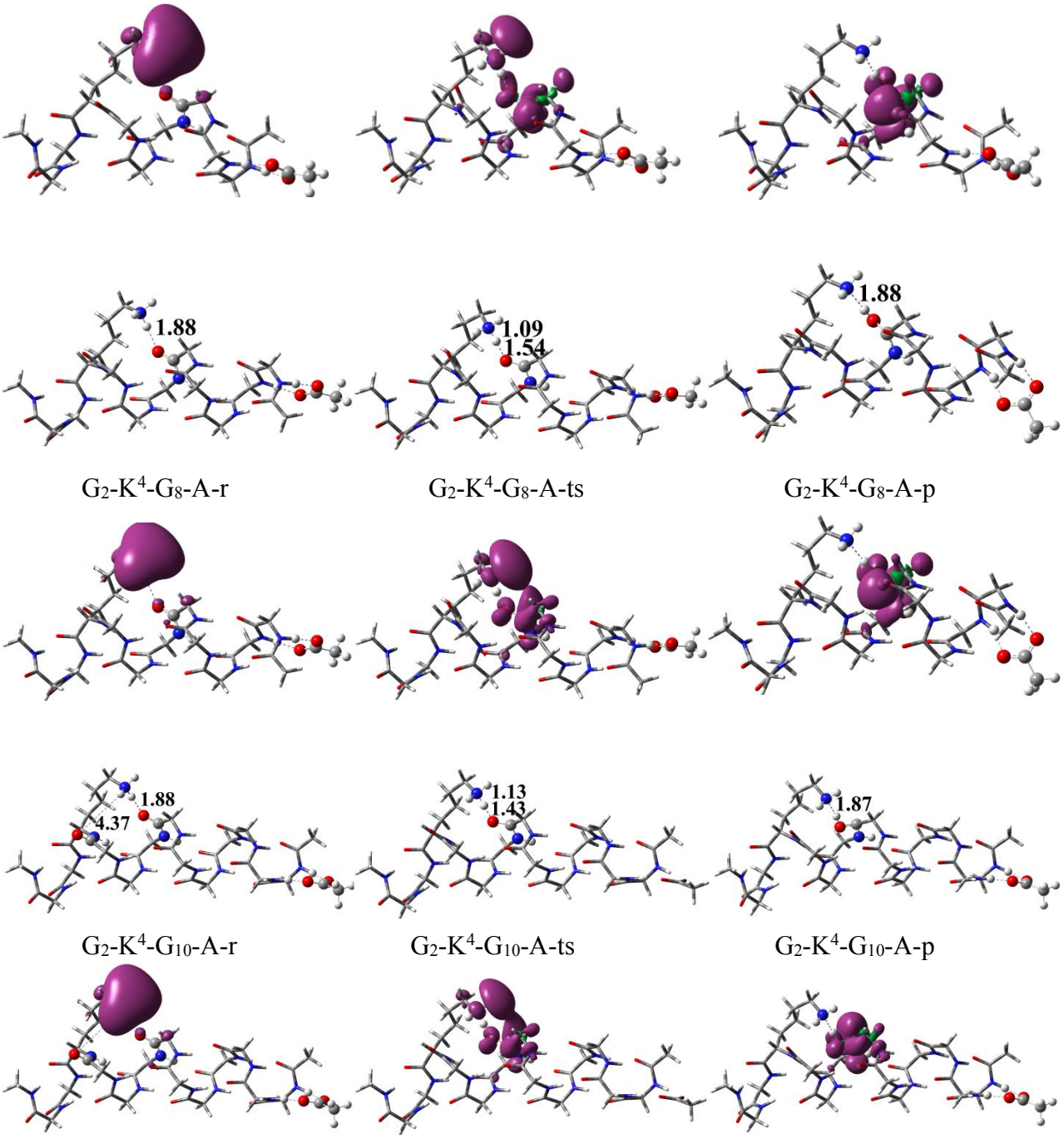

Figure S7. The structures of reactants, transition states, products for G_2-K^4-G_{n-3}-A (n=8, 9, 11, 13) and the corresponding distributions of spin densities for the initial structures with the ammonium group interaction with the helical framework via a hydrogen bond. According these cases, we examined the influence of the capping (the negative groups including the side chains of Asp, Glu) on the PCET reactions in the G_2-K^4-G_{n-3} systems obtained at the B3LYP/6-31+G(d,p) level of theory.

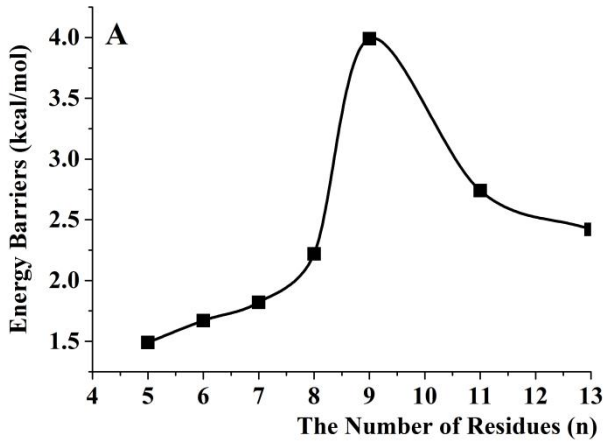

Figure S8. The forward energy barrier of the PCET reactions changes with increasing the number of residues in the G_2-K-G_{n-3} systems (n =5-13). It clearly shows that the forward energy barrier slightly increases with the increasing residues in the helix when n is less than 9 and decreases when n is more than 9.

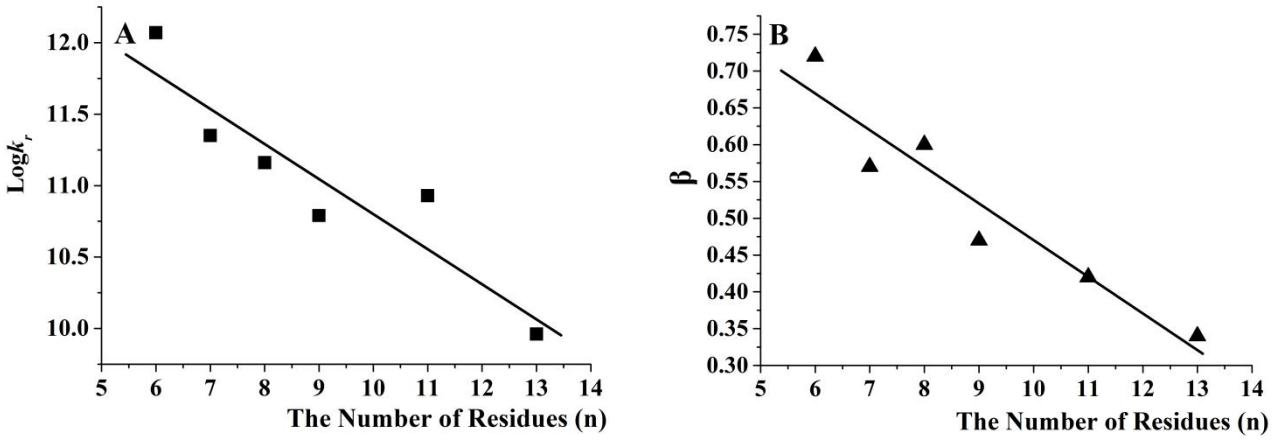

Figure S9. The changing tendences of log(k_r) (A) and the decay factor (β) (B) of electronic coupling matric element (H_{AD}) with increasing residues for the PCET reactions of the G_{n-3}-K-G_2 systems. The slope magnitude of the log(k_r) vs the number of residues (n) in α-helixes is -0.25, indicating the rate constant of PCET is of a shallower dependence on the on the residue number in the α-helix. "B" exhibits the slope magnitude of the electronic coupling attenuation parameter (β) with the number of residues in α-helixes is -0.05, reflecting that longer α-helix is favorable for the PCET reaction.

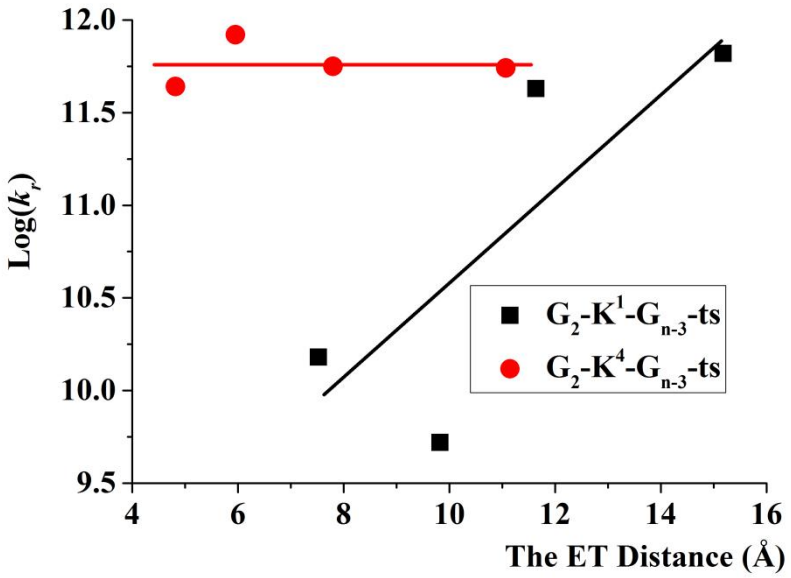

Figure S10. The changing tendence of log(k_r) with the increase of the ET distance for the two-H-binding conformation via G_2-K^1-G_{n-3}-ts and G_2-K^2-G_{n-3}-ts in the G_2-K-G_{n-3} systems.